JOURNAL OF SYNCHROTRON RADIATION

ISSN 1600-5775

Fast beam monitor diamond-based devices for VUV and X-ray synchrotron radiation applications

Michele Di Fraia,[a,d]* Antonio De Sio,[b]† Matias Antonelli,[a] Renzo Nesti,[c] Dario Panella,[c] Ralf H. Menk,[a] Giuseppe Cautero,[a] Marcello Coreno,[a,d] Daniele Catone,[d] Nicola Zema,[d] Carlo Callegari[a] and Emanuele Pace[b]

[a]Elettra – Sincrotrone Trieste S.C.p.A., Basovizza, Trieste, Italy, [b]Dipartimento di Fisica e Astronomia, Universitá di Firenze, Firenze, Italy, [c]Istituto Nazionale di Astrofisica, Osservatorio Astrofisico di Arcetri, Firenze, Italy, and [d]CNR–ISM, Area della Ricerca di Roma Tor Vergata, Roma, Italy. *Correspondence e-mail: michele.difraia@elettra.eu

Received 16 October 2018
Accepted 16 January 2019

Edited by S. Svensson, Uppsala University, Sweden

† Deceased.

This work is dedicated to the memory of Antonio De Sio.

Keywords: CVD diamond; synchrotron; instrumentation; beam monitor; detectors.

The improved performance of third-generation light sources and the advent of next-generation synchrotron radiation facilities require the use of extremely precise monitoring of the main photon-beam parameters, such as position, absolute and relative intensity, and temporal structure. These parameters, and associated real-time feedbacks, are fundamental at the beamline control level and at the machine control level, to improve the stability of the photon beams and to provide bunch-to-bunch quantitative information. Fast response time, high radiation hardness and visible–blind response are main features of photon-beam monitors for VUV and X-ray synchrotron radiation beamlines; hence diamond-based detectors are outstanding candidates. Here, results are presented of an extensive measurement campaign aiming at optimizing the capabilities of diamond detectors to discern time structures below the 100 ps timescale. A custom-built device has been fabricated and tested at the Italian Synchrotron Radiation Laboratory Elettra in Trieste. The results obtained show that diamond is an excellent material for ultra-fast photon pulses with picosecond time resolution; finally the possibilities for application at free-electron laser sources are discussed.

1. Introduction

High-brightness beamlines based on undulator insertion devices are the most sensitive to the electron beam oscillations typical of third-generation synchrotron radiation sources. Therefore, the issue of electron beam stabilization has been extensively addressed in the past years through the development of a fast orbit feedback (FOFB) based on electron beam-position monitors (eBPMs) (Galimberti *et al.*, 2001). Photon beam-position monitors (pBPMs) provide such control systems with additional important information: photon beam position and absolute intensity (Bergonzo *et al.*, 2000; Menk *et al.*, 2007; Pomorski *et al.*, 2009; Feng *et al.*, 2011; Di Fraia *et al.*, 2013; Antonelli *et al.*, 2014); and integration of pBPM information into the FOFB was recently proposed (Fischetti *et al.*, 2002; Morse *et al.*, 2010; Antonelli *et al.*, 2014; Cheng *et al.*, 2018; Sereno *et al.*, 2018).

Although beamlines are generally not provided with a fast local control system based on the information collected by the pBPMs, several beamline experiments require these data to be known for post-processing of the experimental data. As an example, diamond-based solid state detectors applied to X-ray absorption spectroscopy experiments have significantly improved the capabilities of standard spectroscopic techniques (De Sio *et al.*, 2007, 2008). Finally, fourth-generation

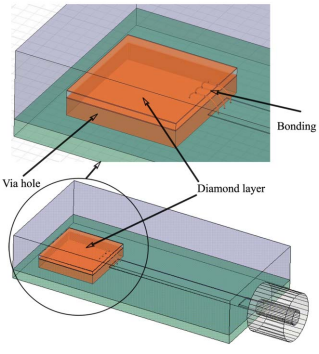

sources also need novel concepts of *in situ* beam diagnostics to keep their high-power photon beams under control. Thus, for both diagnostics and calibration purposes, several synchrotron radiation and free-electron laser (FEL) applications require *in situ* detectors featuring fast response and homogeneity, as well as high radiation hardness to cope with the high dose rates that are typically encountered.

Diamond is an outstanding material for the production of semitransparent *in situ* pBPMs (De Sio *et al.*, 2008; Bergonzo *et al.*, 2006). In a previous campaign, the device presented here was used as a pBPM exhibiting an excellent resolution in the position encoding of 150 nm (Di Fraia *et al.*, 2013; Antonelli *et al.*, 2014). Because of its high bond energy, it can withstand high thermal and radiation loads; its low atomic number makes it semi-transparent under certain combinations of thickness and photon energy. Moreover, due to its high energy gap, intrinsic diamond is an insulator with low thermal noise at room temperature, while its high electron–hole mobility allows charge to be collected faster than in most other material. Such characteristics also make diamond the most interesting material to be used as a pBPM for VUV and X-ray FEL radiation sources (Feng *et al.*, 2011; Antonelli *et al.*, 2012, 2013; Roth *et al.*, 2018), which produce short, intense photon pulses with gigawatt peak power.

We have developed and tested monitor devices based on single-crystal chemical-vapour-deposited (CVD) diamonds with VUV synchrotron radiation light by using radiofrequency (RF) readout electronics. The use of single-crystal diamond detectors for RF time-resolved measurements is a rather new topic and, to our knowledge, this is the first work tackling rigorously the design of a device and adapting the geometry and the impendence of the electric circuit that hosts the detector in order to preserve the shape of the charge pulses and the associated information. The main challenge is to prevent impedance mismatches in the RF signal path, which cause signal reflections. In the following sections we present the design of the structure, the working principle of the detector, and the experimental setup (Section 2), the most significant experimental results (Section 3) and considerations for future work (Section 4).

2. Device concept and experimental setup

Time-resolved beam intensity monitors for VUV and X-ray applications for synchrotron radiation applications require active materials exhibiting low noise, fast response time, radiation hardness and RF readout chains free from signal reflections. To this end we choose diamond as active material and we designed an impedance-matched circuit mount and housing.

The detector has been fabricated starting from a commercial, standard-quality freestanding, 500 µm-thick, single-crystal CVD diamond layer with an area of about 5 mm × 5 mm. Cr–Au contacts were deposited by standard thermal physical vapour deposition; the front electrode has been segmented into four quadrants separated by a clear cross-shaped area (width of the cross arms: 70 µm) to allow the radiation to interact directly with the bulk of the diamond and for future beam-positioning purposes. Free charges are collected by applying a voltage. Each quadrant can be read independently, or the contacts can be shorted together to form a single pixel.

The diamond-based sensor must to be mounted on a microstrip circuit, designed to provide the best performance at high frequencies. When dealing with signals in the microwave range, particular care must be paid to designing the microstrip circuit; wave propagation effects due to the geometry of the surrounding materials must be carefully considered, in order to preserve the proper shape of the waveform.

The whole housing, including the microstrip and the sensor itself, needs to be accurately modelled from an electromagnetic point of view. The use of simplified lumped-element or transmission-line circuit analysis techniques is not sufficient: a full 3D simulation must be performed. A sketch of the electromagnetic model of the diamond-based device is shown in Fig. 1. In order to validate the computer simulation, extensive test measurements need to be carried out, by using a Vector Network Analyzer (VNA), to check scattering parameters. Since very stringent mechanical tolerances are needed, due to the high precision required in the geometry of the housing structure and the connector placing, particular care must also be taken into account in mechanical engineering and prototyping.

In order to maximize the performance in the transduction into a RF signal of a pulsed signal generated by detection of a

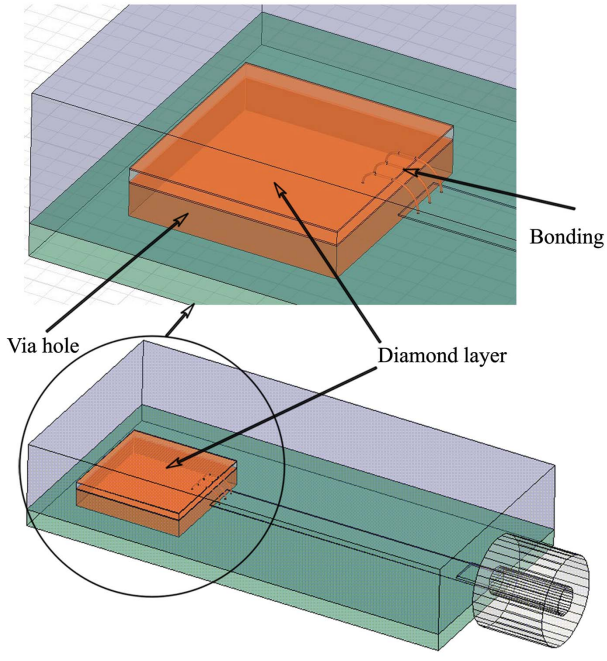

Figure 1
Electromagnetic model of the custom-built diamond-based device. The diamond substrate is electrically connected to a 50 Ω matched copper microstrip (thickness 35 µm) by means of 25 µm wire bonds. The signal output is made by an SMA connector. The dimensions of the device are 20 mm × 10 mm × 4 mm.

fast-changing pulsed photon flux, the detector design has been optimized by using electromagnetic finite-element software. The microstrip device hosting the sensitive diamond chip has been simulated in the time and frequency domains (TD and FD) by using ANSYS *HFSS* (*High-Frequency Structure Simulator*) (ANSYS-HFSS, 2018). Such an accurate analysis is fundamental to predict the impedance matching (FD characterization) along the whole chain following the device and therefore the shape of the output pulsed signal (TD characterization).

At a first stage, a simulation of the scattering parameters of the microstrip circuit and SMA connector (without the diamond substrate) was performed showing, in particular, an excellent reflection coefficient S_{11} always less than −24 dB over a frequency range up to 5 GHz. At a second stage, by analyzing the electromagnetic field of the whole device (diamond substrate, wire bondings, microstrip and SMA connector) and by observing the reflection coefficient S_{11} at the SMA connector port we are able to predict possible matching problems, if any. As shown in Fig. 2, the amplitude and phase curves are a clear indication of a clean single open circuit constituted by the diamond chip, reflecting back all the incoming signal from the microstrip. No multipath reflections are present meaning that all the other parts show good matching and that in the operative environment the diamond sensor will transduce the incident photon radiation to a radio signal, behaving as a high-impedance source and feeding the electrical circuit with no spurious reflections. The microstrip has been embedded into a shielded housing provided with an aperture, that allows the radiation to reach the sensor. A commercial Bias-Tee (PicosecondPulseLab Bias-Tee Mod 5531) has been used to decouple the high-voltage supply from the photo-generated RF signal.

The electromagnetic performance of the circuit has been tested at the radio laboratory of the Arcetri Observatory by using an Anritsu 37277C VNA, which covers a frequency range up to 40 GHz.

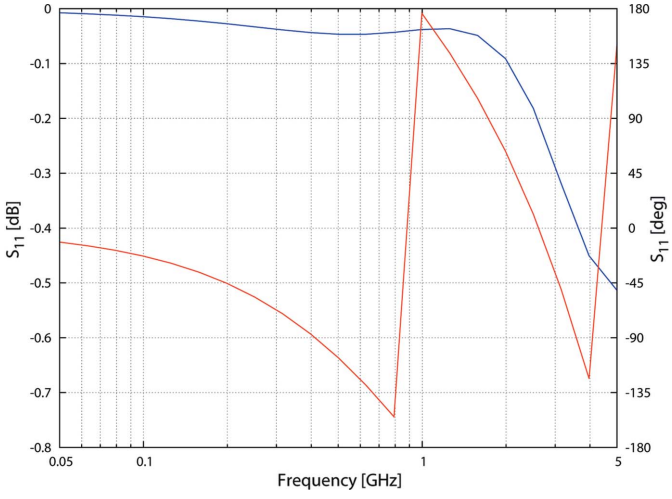

Figure 2
Bode plot of the reflection coefficient S_{11} (blue: amplitude; red: phase) of the device model shown in Fig. 1 up to 5 GHz.

2.1. Experimental setup

The electro-optical characterizations have been carried out at the Italian Synchrotron Radiation Facility – Elettra in Trieste. All measurements have been carried out at the Circular Polarization Beamline (CiPo) that can deliver radiation in the 40–1000 eV spectral range (Derossi *et al.*, 1995). The photon beam has been optimized with a Padmore-type spherical grating monochromator and two vertical slits, to maximize the intensity and minimize the dimension of the photon spot onto the device position. The photon energy was centred around 70 eV with a spot size of 200 µm × 200 µm; the beam intensity was adjusted via the photo-current generated on one of the gold-coated mirrors of the photon transport line. The diamond-based microstrip detector has been settled into a vacuum endstation directly connected to the beamline. The RF signal was then extracted in air through a shielded SMA electrical feedthrough; the device has been biased up to 500 V. The readout has been carried out connecting the output from the Bias-Tee directly (without an intermediate amplification stage) to a Tektronix DP071254 12 GHz 50 GS/s oscilloscope for a first measurement session and later via a 8 GHz 32 dB amplifier to a Tektronix DP073304DX scope with 33 GHz of analog bandwidth and 100–50 GS/s (sampling rate at 2–4 channels). The two different sets of measurements rule out the presence of a signal-shaping contribution from the readout chain.

3. Results

The Elettra storage ring standard (multibunch) operation mode consists of 432 buckets, spaced by 2 ns. Our measurement required a finely time-structured photon beam; thus we requested dedicated beam time with a hybrid mode filling pattern of the storage ring. In such a configuration most of the 432 buckets are uniformly filled with electrons, with the exception of an empty gap, of about 40 buckets, called the dark gap (DG), in which a single, more intense, electron bunch (about 4 mA) called the hybrid peak (HP) is injected. The synchrotron was operated in 'top-up' mode, where a regular injection of current of 1 mA every 20 min (beam lifetime = 40 h) occurs in order to compensate for charge losses (see Fig. 3).

Inside the undulator (in our case that of the CiPo beamline) each electron bunch generates a radiation beam with a time structure that reflects the density distribution of the bunch itself.

In a previous calibration of the synchrotron time structure, in the same operational mode, a time width of each pulse between 150 ps and 200 ps has been found by means of a streak camera (Hamamatsu-Photonics, http://www.hamamatsu.com).

This operation mode is then ideal to test the performance of the detector in discriminating time-resolved structures. The isolated HP allows: to verify the capability of reproducing the same features of the bunch, to check the rise and fall times, and to assess the signal ground level (in the DG) where no

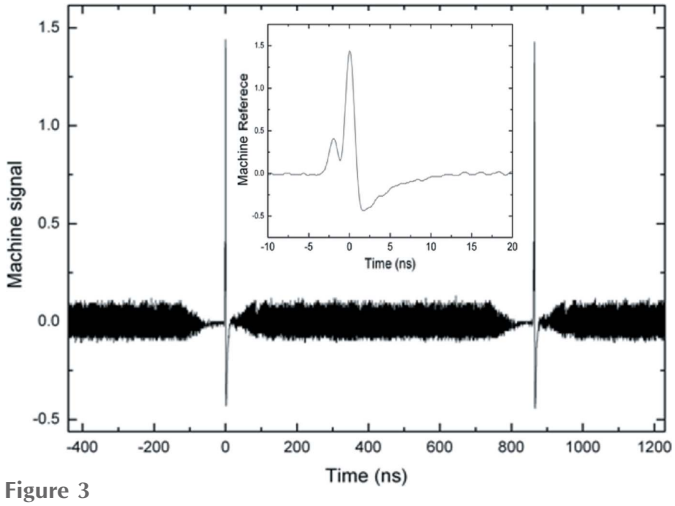

Figure 3
Time structure of the distribution of bunches within the synchrotron storage ring measured with a conventional electron beam-position monitor (eBPM). Inset: magnification of the hybrid peak within the dark gap.

signal is expected. Using the multi-bunches train of pulses we could verify: that the detector can clearly separate one pulse from the next and that the electrical signal recovers to ground level in between. The overall time structure of the signal is shown in Fig. 3 as recorded by an eBPM present in the storage ring of Elettra. All the negative undershoots are due to the signal shaping of such a detector, as shown by the inset showing a zoom over the HP region. Consultation with Elettra's control room provided mutual feedback on bunches distribution status. Such a procedure has revealed a partial filling of the bucket preceding the HP as evident in the inset of Fig. 3.

3.1. Detector

At the maximum sampling rate available with the Tektronix DP073304DX oscilloscope it is possible to record two revolutions within a single sweep, as shown in Fig. 4. It is possible to observe the same time structure recorded with the eBPM. However, our detector shows a well defined dark (ground) level of the signal, that is the same for the dark gap as for the multi-bunch train. That indicates the capability to separate the contribution from single peaks, which can be confirmed by expanding the temporal scale in the multi-bunch train (Fig. 5), where all peaks are well defined, evenly separated, and exhibit fast rise and decay times.

The ground level is not affected by the bias, so we can presume that the noise observed is due not to the detector but to the readout chain (insulated by the Bias-Tee). Indeed the ground-level noise (0.05 mV r.m.s.) is comparable with the noise of the oscilloscope input stage. The ground level is recovered between the peaks in the multi-bunch zone, meaning that the 2 ns spacing between two consecutive peaks is enough for the detector to collect all the photo-generated charges. This confirms the quality of design of the RF-matched device, and the limited influence of trapping/de-trapping processes, which is a known cause of the persistence of

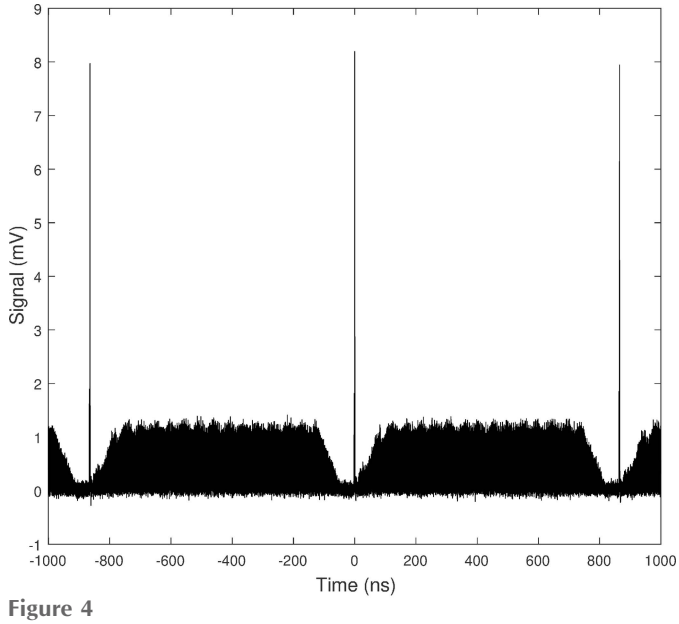

Figure 4
As Fig. 3, measured with the diamond-based detector and the Tektronix DP073304DX oscilliscope. More than two full machine periods can be recorded at once.

photoconductivity for this kind of detector (Marinelli *et al.*, 2001; Balducci *et al.*, 2005).

An in-depth analysis of the isolated HP has been carried out at different biases (from 50 V up to 500 V) to characterize the detector performance. Many waveforms have been acquired for each bias in order to have a statistically relevant set of measurements. The above-mentioned spurious filled bucket preceding the HP does not affect our analysis since the two are separated enough.

The HP has been analysed by fitting it with a multi Gaussian function (corresponding to the shape of the emitting electrons bunch, see Fig. 6). One Gauss curve is sufficient to fit the peak with a good confidence level, confirming the absence of signal

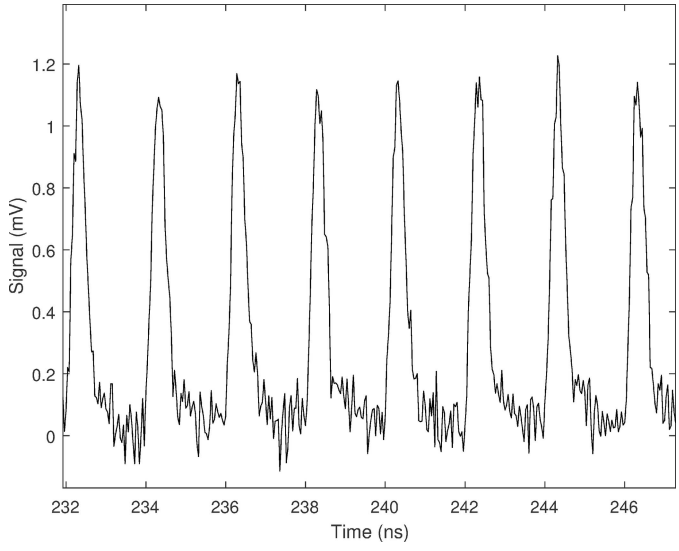

Figure 5
Zoom in of Fig. 4 in the multi-bunch region, showing the clearly resolved individual peaks.

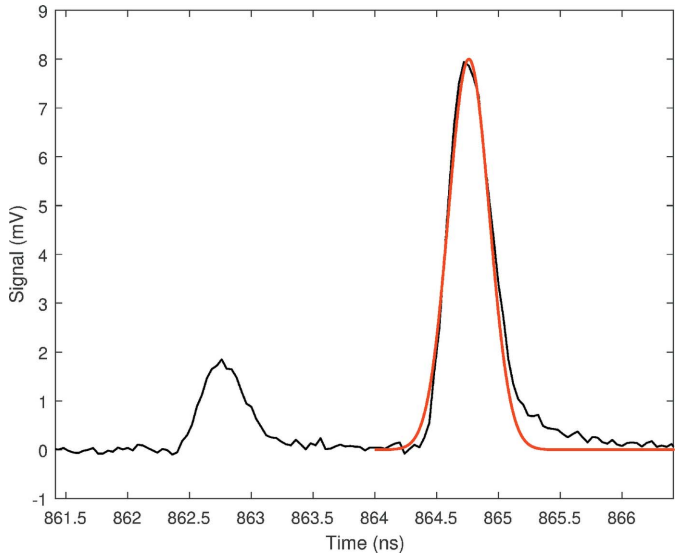

Figure 6
Zoom in of Fig. 4 in the hybrid peak region (black) and Gaussian fit of the main peak (red). The best-fit value of the FWHM is 389 ps. A rise time of 186 ps has been estimated from the experimental curve.

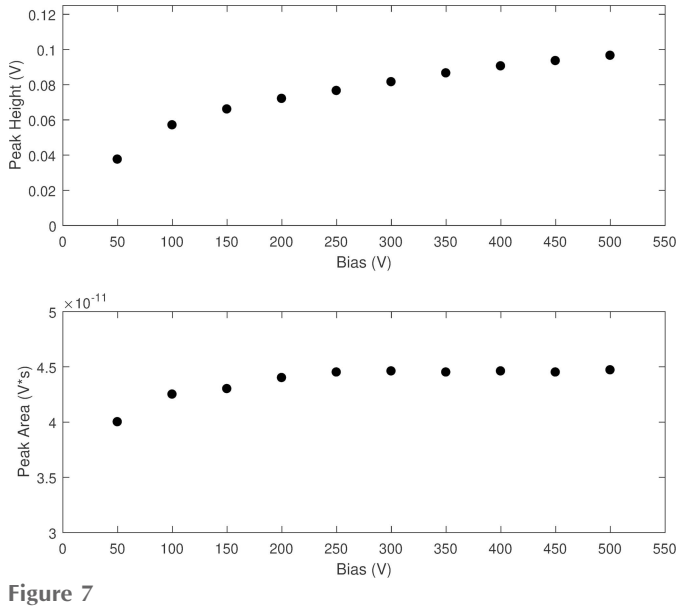

Figure 7
Best-fit parameter distribution. Top: height of the hybrid peak at different bias voltages. Bottom: area of the hybrid peak at different bias voltages.

reflections characteristic of impedance mismatch between the detector and the read-out system.

The residual error between the fit and the experimental data lies in the small asymmetric tail on the trailing edge of the peak, which is probably due to the relaxation of charges into the diamond device or to a negligible fast de-trapping process after the exciting pulse. Specific peak features have been analysed in order to provide simultaneous information on the detector performance, and on the electro-optical properties of the diamond composing the sensitive chip. In particular, the distribution of parameters (height, area, FWHM and rise time) of a Gaussian fit of the HP for increasing bias voltages is shown in Figs. 7 and 8.

From a physical point of view, each photon pulse generates a volume of charges into the diamond. The amount of charge detected by the contacts and the time required to collect such charge depends on the properties of the material and on the detector design. The peak area depends on the total amount of carriers detected, and can be thus correlated with the charge collection efficiency at the electric contact. The FWHM depends on the time required to collect the charge at the contact, giving information on mobility and drift velocity inside the material. The peak height depends on both of these factors. Note that FWHM and peak height can be affected by the impedance coupling of the detector with the readout system and by the overall resulting bandwidth of the system itself. The rise time of the peaks is mostly influenced by the velocity of the carriers into the diamond and by the bandwidth, much less by reflections that produce 'afterimages signals' and make the peak wider and asymmetric on the trailing edge. The comparison between the peak height and the rise time can give a qualitative idea of the presence of impedance coupling.

In Fig. 7 the peak area increases steeply, with the applied bias, reaching a saturation value at about 200 V. That implies

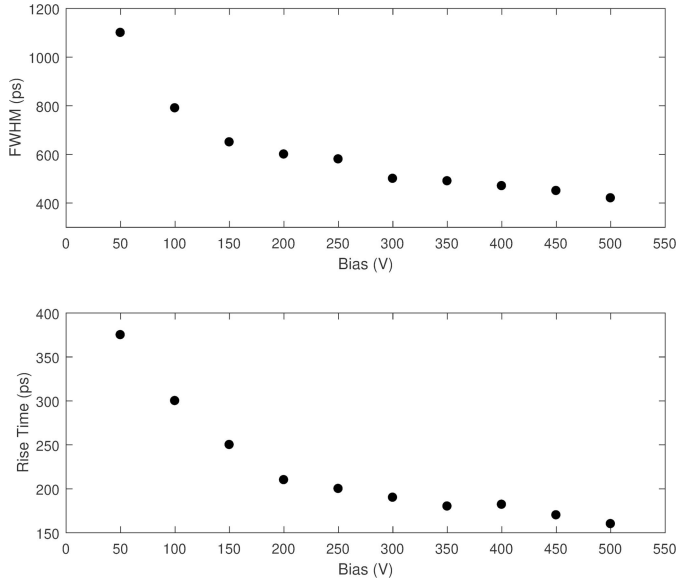

Figure 8
Best-fit parameter distribution. Top: FWHM of the hybrid peak at different bias voltages. Bottom: rise time (see text for details) of the hybrid peak at different bias voltages.

that for applied biases $V \geq 200$ V almost all the photogenerated charges are collected. In terms of material properties the saturation of the collected charges implies that the collection distance L, specifically for photoconductors, $L = \mu\tau E$ (where μ is the carrier mobility, τ is its lifetime, E is the electric field), becomes greater than the distance between the contacts, and all the charges reach their corresponding contact.

On the other hand, as one can see from the top panel of Fig. 7, the peak height monotonically increases with increasing bias and no evident saturation level is reached at 500 V. This implies that the drift velocity $D = \mu E$ of the carriers into the

material has not being saturated. Since the saturation of the drift velocity is associated with the interaction with defects and with the lattice structure, this confirms the good quality of the selected single-crystal diamond substrate.

It is clear from the above that the peak width has to decrease monotonically even for values greater than 200 V, down to 400 ps at 500 V (see Fig. 8). As shown in Fig. 8, the time performance of the device improves rapidly with the bias as the rise time and the FWHM decrease. Nevertheless, the minimum values reached at 500 V, 186 ps for the rise time and 389 ps for the FWHM, are greater than the width estimated with the streak camera (at worst 200 ps). These limits of the device performance require a deeper analysis to be understood, and will be discussed in the following section.

Even if the limits of the electron bunch time width are not reached, the detector performance is sufficient to give precise information on the bunches and can be used to give real-time feedback on the machine status to the control system of the storage ring and to the experiments performed at the beamlines.

We stress that the peaks' shapes and the correlation coefficients of Gaussian fits confirm the absence of mismatch losses or reflected signals.

4. Summary and future perspectives

A diamond device integrated into an adapted 50 Ω matched microstrip circuit has been designed and fabricated. Preliminary in-laboratory characterizations have been carried out to confirm the design quality. Characterization measurements have been performed at the CiPo beamline of the Italian Synchrotron Facility – Elettra. The good impedance matching has been shown by the absence of spurious reflected signals. Measurements aimed at characterizing the detector performance have been carried out as a function of the applied bias and a detailed analysis has been performed. Even if the thickness of the diamond active material had not been optimized for such application, the detector speed and charge collection efficiency turned out to be excellent. The time resolution seems to be significantly limited not by the overall bandwidth of the readout system but by the sensitive part of the detector itself. New contact design and optimization of the diamond plate thickness have to be taken into consideration to further improve the device capabilities to measure time features of photons peaks shorter than 400 ps. Our detector works in sandwich configuration, therefore the bias is applied between a back and a front electric contact and the electric field is perpendicular to the top surface of the diamond chip. Thus in order to improve the detector time resolution we can think to two different scenarios:

(i) Whenever the radiation is absorbed just below the front surface (this depends on the sensitive-material properties and on the radiation energy, in our case the absorption length in diamond at 70 eV photon energy is 55 nm) a coplanar geometry is preferred. In such a configuration both electric contacts are deposited on the front surface, with geometries that maximize the contact surface while minimizing the distance between the contacts. With respect to the presented geometries, we should expect that the electric field (*i.e.* the component parallel to the surface), responsible for the charge collection, increases several times allowing such time performance to be reached.

(ii) Whenever the radiation is more penetrating into the material we can reduce the time required to collect the carriers by reducing the thickness of the detector, so that we can expect to increase the overall time resolution of the detector. As an example considering the following equation for the drift velocity, $v_d = \mu E/[1 + (\mu E/v_s)]$, where v_s is the typical velocity saturation value in diamond ($v_s = 10^7$ cm s^{-1}) and with a typical carrier (holes) mobility of $\mu = 2100$ cm s^{-1}, the saturation of the drift velocity occurs with electric fields $E > 24$ kV cm^{-1} (Oshiki *et al.*, 2006). Thus the expected transit time $t_r = L/\mu E$ of the charges for $L = 20$ µm-thick diamond substrate is 40 ps. Note that this is a rough estimate, not taking into account possible trapping/de-trapping processing or lattice defects.

In summary, upon decreasing the thickness of the diamond substrate, we expect that the proposed device will be capable of resolving the temporal duration of each single synchrotron radiation pulse; further investigations will be performed in this direction.

In addition, we think that such a device might be promising also for FEL applications. Provided that no signal reflections are present in the readout chain, as our device demonstrates, combined with the excellent linearity that such devices exhibit over a wide range of intensities (De Sio *et al.*, 2008; Keister & Smedley, 2009; Smedley *et al.*, 2011; Roth *et al.*, 2018), and considering the positive results obtained as pBPM (Antonelli *et al.*, 2012), we believe that such devices can be used for discriminating single FEL pulses even at high repetition rate, although without resolving the temporal width of a single sub-100 fs FEL pulse.

Acknowledgements

We gratefully acknowledge Sandro Rinaldi, Carlo Spezzani, Luca Cresci, Stefano Krecic and Emmanuel Karantzoulis for their valuable support.

References

ANSYS-HFSS (2018). *3D Electromagnetic Field Simulator for RF and Wireless Design*, https://www.ansys.com/it-it/products/electronics/ansys-hfss.

Antonelli, M., Cautero, G., Cudin, I., Eichert, D. M., Giuressi, D., Jark, W. H., Karantzoulis, E., Lizzit, S., Menk, R. H., De Sio, A., Pace, E. & Di Fraia, M. (2014). *Proceedings of the 5th International Particle Accelerator Conference (IPAC2014)*, 15–20 June 2014, Dresden, Germany, pp. 3341–3343. THPME128.

Antonelli, M., Di Fraia, M., Carrato, S., Cautero, G., Menk, R., Jark, W., Ganbold, T., Biasiol, G., Callegari, C., Coreno, M., De Sio, A. & Pace, E. (2013). *Nucl. Instrum. Methods Phys. Res. A*, **730**, 164–167.

Antonelli, M., Di Fraia, M., Tallaire, A., Achard, J., Carrato, S., Menk, R. H., Cautero, G., Giuressi, D., Jark, W. H., Biasiol, G., Ganbold, T., Oliver, K., Callegari, C., Coreno, M., Sio, A. D. & Pace, E. (2012). *Proc. SPIE*, **8504**, 85040D.

Balducci, A., Marinelli, M., Milani, E., Morgada, M. E., Prestopino, G., Scoccia, M., Tucciarone, A. & Verona-Rinati, G. (2005). *Appl. Phys. Lett.* **87**, 222101.
Bergonzo, P., Brambilla, A., Tromson, D., Mer, C., Hordequin, C., Guizard, B., Foulon, F., Solé, V. A. & Gauthier, C. (2000). *Diamond Relat. Mater.* **9**, 960–964.
Bergonzo, P., Tromson, D. & Mer, C. (2006). *J. Synchrotron Rad.* **13**, 151–158.
Cheng, W., Bacha, B., Kosciuk, B. & Jr, D. P. (2018). *Proceedings of the 9th International Particle Accelerator Conference (IPAC2018)*, 29 April–4 May 2018, Vancouver, BC, Canada, pp. 1837–1840. WEPAF012.
Derossi, A., Lama, F., Piacentini, M., Prosperi, T. & Zema, N. (1995). *Rev. Sci. Instrum.* **66**, 1718.
De Sio, A., Bocci, A., Pace, E., Castellano, C., Cinque, G., Tartoni, N. & D'Acapito, F. (2008). *Appl. Phys. Lett.* **93**, 083503.
De Sio, A., Pace, E., Cinque, G., Marcelli, A., Achard, J. & Tallaire, A. (2007). *At. Spectrosc.* **62**, 558–561.
Di Fraia, M., Antonelli, M., Tallaire, A., Achard, J., Carrato, S., Menk, R., Cautero, G., Giuressi, D., Jark, W., D'Acapito, F., Sio, A. D. & Pace, E. (2013). *J. Phys. Conf. Ser.* **425**, 212001.
Feng, Y., Feldkamp, J., Fritz, D., Cammarata, M., Robert, A., Caronna, C., Lemke, H., Zhu, D., Lee, S., Boutet, S., Williams, G., Tono, K., Yabashi, M. & Hastings, J. (2011). *Proc. SPIE*, **8140**, 81400Q.
Fischetti, R. F., Heurich, R., Perry, D., Stepanov, S., Kondrashkina, E. & Rosenbaum, G. (2002). *Rev. Sci. Instrum.* **73**, 1518.
Galimberti, A., Borghes, R., Paolucci, G., Presacco, R., Paolicelli, G. & Stefani, G. (2001). *Nucl. Instrum. Methods Phys. Res. A*, **467–468**, 221–225.
Keister, J. W. & Smedley, J. (2009). *Nucl. Instrum. Methods Phys. Res. A*, **606**, 774–779.
Marinelli, M., Milani, E., Paoletti, A., Tucciarone, A., Verona-Rinati, G., Angelone, M. & Pillon, M. (2001). *Phys. Rev. B*, **64**, 195205.
Menk, R. H., Giuressi, D., Arfelli, F. & Rigon, L. (2007). *AIP Conf. Proc.* **879**, 1109–1112.
Morse, J., Solar, B. & Graafsma, H. (2010). *J. Synchrotron Rad.* **17**, 456–464.
Oshiki, Y., Kaneko, J., Fujita, F., Hayashi, K., Meguro, K., Homma, A., Kawamura, S., Yokota, Y., Yamamoto, Y., Kobashi, K., Imai, T., Sawamura, T. & Furusaka, M. (2006). *Diamond Relat. Mater.* **15**, 1508–1512.
Pomorski, M., Ciobanu, M., Mer, C., Rebisz-Pomorska, M., Tromson, D. & Bergonzo, P. (2009). *Phys. Status Solidi A*, **206**, 2109–2114.
Roth, T., Freund, W., Boesenberg, U., Carini, G., Song, S., Lefeuvre, G., Goikhman, A., Fischer, M., Schreck, M., Grünert, J. & Madsen, A. (2018). *J. Synchrotron Rad.* **25**, 177–188.
Sereno, N., Arnold, N. D., Blake, R. W., Brill, A. R., Bui, H., Carwardine, J., Decker, G., Emery, L., Fors, T., Kallakuri, P. S., Keane, R. T., Lill, R. M., Paskvan, D. R., Pietryla, A. F., Shang, H., Sun, X., Veseli, S., Wang, J., Xu, S. & Yang B. X. (2018). *Proceedings of the 9th International Particle Accelerator Conference (IPAC2018)*, 29 April–4 May 2018, Vancouver, BC, Canada, pp. 1204–1207. TUZGBD3.
Smedley, J., Héroux, A., Keister, J. W., Gaowei, M., Muller, E., Brook, S., Bohon, J., Attenkofer, K. & Distel, J. (2011). *Proceedings of the 2011 Particle Accelerator Conference (IPAC2011)*, 28 March–3 April 2011, New York, USA, pp. 483–485. MOP207.